

SlimFL: Federated Learning with Superposition Coding over Slimmable Neural Networks

Won Joon Yun, Yunseok Kwak, Hankyul Baek, Soyi Jung, *Member, IEEE*, Mingyue Ji, *Member, IEEE*, Mehdi Bennis, *Fellow, IEEE*, Jihong Park, *Senior Member, IEEE*, and Joongheon Kim, *Senior Member, IEEE*

Abstract—Federated learning (FL) is a key enabler for efficient communication and computing leveraging devices’ distributed computing capabilities. However, applying FL in practice is challenging due to the local devices’ heterogeneous energy, wireless channel conditions, and non-independently and identically distributed (non-IID) data distributions. To cope with these issues, this paper proposes a novel learning framework by integrating FL and width-adjustable slimmable neural networks (SNN). Integrating FL with SNNs is challenging due to time-varying channel conditions and data distributions. In addition, existing multi-width SNN training algorithms are sensitive to the data distributions across devices, which makes SNN ill-suited for FL. Motivated by this, we propose a communication and energy-efficient SNN-based FL (named *SlimFL*) that jointly utilizes *superposition coding (SC)* for global model aggregation and *superposition training (ST)* for updating local models. By applying SC, SlimFL exchanges the superposition of multiple width configurations decoded as many times as possible for a given communication throughput. Leveraging ST, SlimFL aligns the forward propagation of different width configurations while avoiding inter-width interference during backpropagation. We formally prove the convergence of SlimFL. The result reveals that SlimFL is not only communication-efficient but also deals with the non-IID data distributions and poor channel conditions, which is also corroborated by data-intensive simulations.

Index Terms—Federated learning, Heterogeneous devices, Slimmable neural network

I. INTRODUCTION

A. Background and Motivation

RECENT advances in machine learning (ML) and hardware technologies have pushed deep learning down from cloud servers to edge devices such as phones, cars, and the Internet of things (IoT) devices [2], [3]. These edge devices collectively constitute a source of ever-growing big data, so

are indispensable for training high-quality machine learning models. Meanwhile, each edge device stores only a tiny fraction of the big data, which is often privacy-sensitive (e.g., navigation history, e-Health wearable records, and surveillance camera photos). To exploit these opportunities and address the challenges induced by edge devices, federated learning (FL) is a promising solution that allows edge devices to train a global model by exchanging locally trained models instead of raw data [4]–[7].

At its core, FL operations rest on repeatedly constructing a global model averaged over the local models, which is downloaded by each device to replace its local model with the new global model. By design, FL necessitates the use of a single global model for all devices. This requirement restricts the scalability and accuracy of FL, particularly when scaling to the sheer number of edge devices, which have non-identical memory resources and energy budgets not to mentioned as different communication channel conditions. Therefore, the use of a single large model may be suited for only a few devices, whereas the use of a tiny model should be accompanied by compromising accuracy.

In light of the aforementioned issues in communication-energy efficiencies and scalability, the recently proposed slimmable neural network (SNN) architectures have a great potential in that an SNN can adjust its model width in accordance with its available energy budget or task difficulty. Inspired from this, in this article, we propose an *SNN-based FL algorithm* that makes use of *superposition coding (SC)* and *successive decoding (SD)*, coined *slimmable FL (SlimFL)*. To illustrate the effectiveness of SlimFL, consider an SNN with two width configurations, as seen in Fig. 1. Each device uploads its local updates during the uplink to the server after jointly encoding the left-half (LH) and right-half (RH) of its local SNN model and assigning distinct transmission power levels, i.e., SC [8]. The server then makes an attempt to decode the LH. If the LH is successfully decoded, the server attempts to decode the RH consecutively, i.e., SD, also known as successive interference cancellation (SIC). As a result, when the device-server channel throughput is poor, the server decodes only the LH of the uploaded model, yielding a model with a *half-width (0.5x) width*. When the channel has a high throughput, the server may decode both LH and RH and combine them to produce the *full-width model (1.0x)*. As a result, the server creates a global model superimposing the decoded 0.5x and 1.0x local models, which each device downloads. The device substitutes the downloaded global model for its local model and repeats the preceding step until

Preliminary version of this paper was accepted to IEEE Conference on Computer Communications (INFOCOM), May 2022 [1].

This research is supported by the National Research Foundation of Korea (NRF-Korea, 2021R1A4A1030775) and the Institute of Information & Communications Technology Planning & Evaluation (IITP) grant funded by the Korea government (MSIT) (No. 2021-0-00467, Intelligent 6G Wireless Access System). (*Corresponding authors: Soyi Jung, Jihong Park, Joongheon Kim*)

W. J. Yun, Y. Kwak, H. Baek, and J. Kim are with the School of Electrical Engineering, Korea University, Seoul 02841, Republic of Korea, e-mails: {ywjoon95,rhkrdbstjr0,67back,joongheon}@korea.ac.kr.

S. Jung is with the School of Software, Hallym University, Chuncheon 24252, Republic of Korea, e-mail: sjung@hallym.ac.kr.

M. Ji is with the Department of Electrical and Computer Engineering, The University of Utah, Salt Lake City, UT 84112, USA, e-mail: mingyue.ji@utah.edu.

M. Bennis is with the Centre for Wireless Communications, University of Oulu, Oulu 90014, Finland, e-mail: mehdi.bennis@oulu.fi.

J. Park is with the School of Information Technology, Deakin University, Geelong, VIC 3220, Australia, e-mail: jihong.park@deakin.edu.au.

convergence. In addition, the same technique may be extended to the server-to-device downlink.

SlimFL’s efficacy is contingent upon achieving synergy between several width configurations, namely 0.5x and 1.0x models, which is a difficult task. The existing FL algorithm does not focus on synergetic of 0.5x and 1.0x. In addition, since the local model has various width configurations, training them may conflict with one another. To the best of our knowledge, FL with different width configuration have not been proposed, yet. Existing SNN architectures and training techniques are designed for standalone learning and so are unsuitable for SlimFL, especially when data distributions are not independent and identical (non-IID). To address these issues in SlimFL, we provide a new SNN architecture and training method called *superposition training (ST)*, as well as a study of SlimFL’s convergence and efficiency.

B. Contributions

The major contributions of this paper are summarized as follows.

- We first propose an FL framework for SNNs, SlimFL (see Fig. 1 and **Algorithm 4**), which uses SC for enhancing communication efficiency under time-varying wireless channels with limited bandwidth.
- We develop a local SNN training method for SlimFL, ST (see **Algorithm 3**), which minimizes excessive inter-width interference and achieves fast convergence with good accuracy while being agnostic to data distribution.
- We prove the convergence of SlimFL (see **Theorem 1**). Numerical results show the benefits of SlimFL in terms of channel quality and data distributions and characterizes the optimum transmit power allocation for SC (see **Proposition 1**), and the optimal ST ratio allocation (see **Proposition 2**).
- We verify our analysis via simulations, indicating that SlimFL achieves higher accuracy and lower communication costs than vanilla FL (i.e., FedAvg) under poor channel conditions and non-IID data distributions.

In our previous work [1], we only described the brief idea of SlimFL, and provided the proof sketches of convergence. In this work, we delineate the detailed operations and motivation of SlimFL, while elaborating on the full derivation steps of the convergence proofs. To further advocate the feasibility of SlimFL under various scenarios, we numerically study the impacts of different channel models, datasets, and local training capabilities in Sec. VI-D.

C. Organization

The rest of this paper is organized as follows. Sec. II describes previous research results of FL and background knowledge of superposition coding and successive decoding. Sec. III presents the proposed SNN model and its training method (i.e., SUSTrain), and Sec. IV designs SlimFL using superposition coding and successive decoding, Sec. V shows the convergence analysis on SlimFL. Sec. VI presents the simulation-based performance evaluation and its result regarding SlimFL. Finally, Sec. VII concludes this paper.

The notations used in this paper are listed in Table I.

TABLE I
LIST OF NOTATIONS

Symbol	Description
K	The number of devices
T	Total iteration step
S	The number of width configurations in SNN
θ^G	Parameter of global model
θ^k	Parameter of k -th local model
Ξ_i	Binary mask to extract model parameter of i -th model
Ξ	Binary mask to extract model parameter of LH segment
Ξ^{-1}	Binary mask to extract model parameter of RH segment
H	Set of successfully decoded LH segment
F	Set of successfully decoded RH segment
n_L	The number of successfully decoded LH segment
n_R	The number of successfully decoded RH segment
p_i	Decoding success probability of i -th message
Z	Entire dataset
ζ_t^k	Local data sampled from k -th device at t
w_i	Ratio of superpositioned training for updating i -th model
λ	Power allocation ratio
η_t	Learning rate of t
\odot	Element-wise multiplication
$M(\theta_t^k, \zeta_t^k)$	Logits from feed-forwarding ζ_t^k to k -th SNN
$y(\zeta_t^k)$	Ground truth of ζ_t^k
γ	Signal-to-interference-plus-noise ratio (SINR)
σ^2	Noise power
d	Distance between the local device and the server
β	Pathloss exponent
P	Transmit power
P_I	Interference power
u	Code rate
χ	Small-scale fading
R	Received throughput

II. RELATED WORKS

A. Efficient Artificial Intelligence

It is customary to prune model parameters to satisfy varying on-device energy and memory limits [9] or to distill the knowledge of a big trained model into a small empty model through knowledge distillation (KD) [10], but this requires extra training operations. Alternatively, one may alter the width and/or depth of a trained model to match the resource needs. After training, depth-controlled neural networks [11] and adaptive neural networks [12] can modify their depths, while SNNs alter their widths [13]. According to studies [13]–[15], many SNN architectures and their algorithms are proposed. The authors of [14] first propose SNN with existing neural networks (e.g., MobileNet-v1, MobileNet-v2, ShuffleNet, and ResNet50). Then, the authors of [13] enhances existing SNN with batch normalization (BN), sandwich rule and inplace distillation. In [15], SNN is extended to make a decision on how hard an input image is to classify using sandwich gate sparsification. The nowadays trend of SNN studies is to implement the concept of SNN in specific research areas (e.g., computer vision [16], wireless communication [1], speech recognition [17] or signal processing [15]).

B. Federated Learning

In FL, each edge device trains its model with its own data. After training, all parameters of each local model is

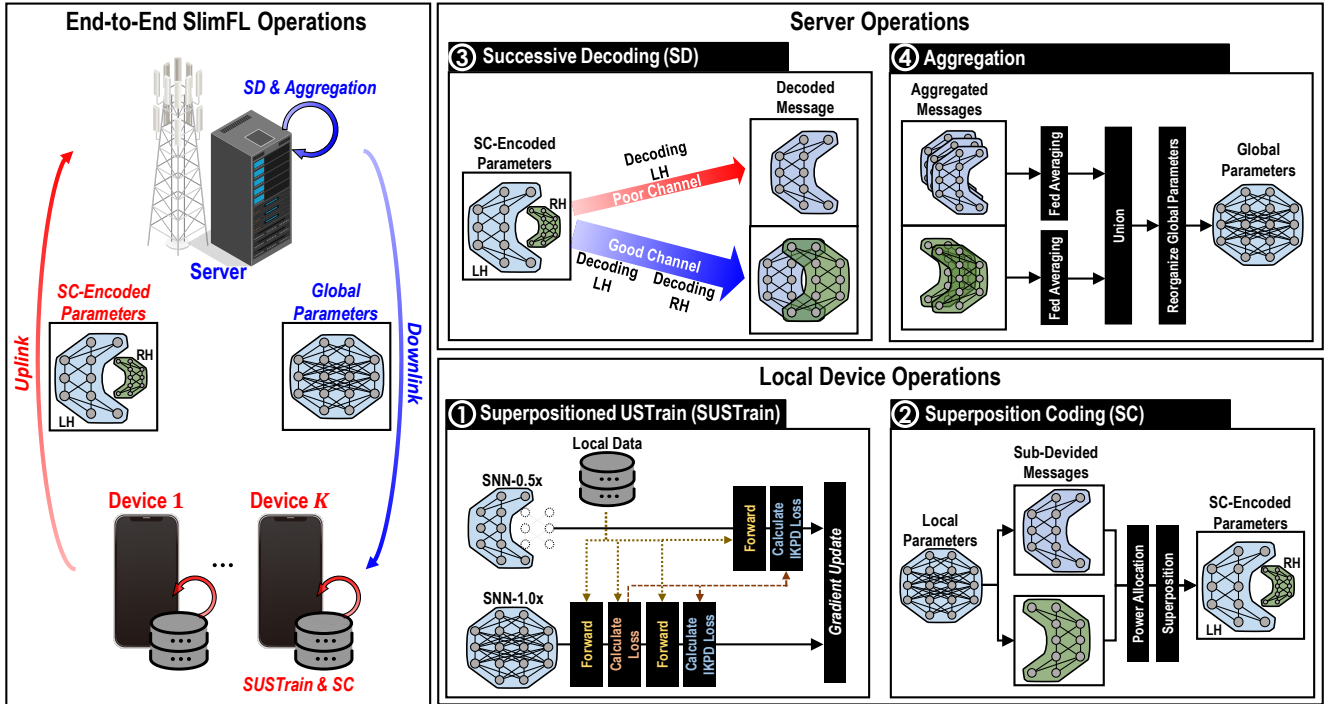


Fig. 1. A schematic illustration: SlimFL consists of four processes. On the local side, the local SNN is trained with SUSTrain. After training, the local SNN is coded with SC. The local devices transmit SC-encoded local parameters to the server. On the server-side, the server successively decodes SC-encoded parameters. The server aggregates the decoded parameters and reconstructs the global parameters.

transmitted to the server (e.g., cloud, fog, or edge). The server reconstructs the global model by aggregating the local model parameters. Here, FL is privacy-preserving because the device does not transmit its own data to the server.

1) Challenges of Communication and Computing Costs:

Although FL has advantages regarding privacy-preserving, there are many issues on FL such as communication/computing costs due to non-IIDness. To reduce those costs, many FL algorithms have been supposed. Federated Averaging (FedAvg) is a solution that the global model is obtained with averaging local model parameters [4]. FedAvg reduces 10-100x of communication costs compared to the existing FL algorithm [18]. In addition, FL with local batch normalization (FedBN [19]) or FL with a generalization and re-parametrization (FedProx [20]) improves the speed of convergence of the FL regime, which means reducing more communication/computing costs. In this paper, we leverage width-controllable SNNs, and develop its FL version, SlimFL. Such an extension is non-trivial, and entails several design issues, such as local SNN training algorithms, aggregating segment prioritization.

2) *FL Convergence Analysis:* FL convergence has been extensively studied [21], [22], and this study depends on the following convergence studies. Vanilla FL, also known as FedAvg, is equivalent to the well-known local stochastic gradient descent (SGD) method for IID data distributions [23]. FedAvg convergence is offered for non-IID data distributions [24], where non-IIDness is defined as the constraint on dissimilarity between global and local average risks. Alternatively, the authors of [22] develop the convergence analysis under

non-IID data distributions, where non-IIDness is quantified by the average of the local stochastic gradient variance across devices. When considering non-IID data distributions, our SlimFL convergence study is essentially based on the approach described in [24], while our concept of non-IIDness is comparable to [22]. Notably, the convergence of standalone SNN training has been explored lately [25], albeit without the use of FL.

C. Superposition Coding & Successive Decoding

As shown in Fig. 1, SC compresses two distinct data signals into a single one while assigning two distinct power levels prior to transmission [8]. SD decodes the SC-encoded signal after receptions by decoding the stronger signal first, removing it, then decoding the remaining as the weaker signal [26]. SC is frequently used in communication systems, most notably for supporting multiple devices concurrently in the context of non-orthogonal multiple access (NOMA) [27], [28]. We use the same principle to support a single device that simultaneously requests two different types of data with different priorities, such that the higher priority signal is almost always decoded first, while the lower priority signal can be decoded sequentially only under favorable channel conditions. To be precise, SlimFL prioritizes an SNN's LH in order to obtain the 0.5x model even across inferior channels. It is capable of decoding the RH of the SNN only when the channel circumstances are favorable, yielding the 1.0x model by merging both LH and RH. As a result, SlimFL provides consistent convergence even in the presence of weak channels.

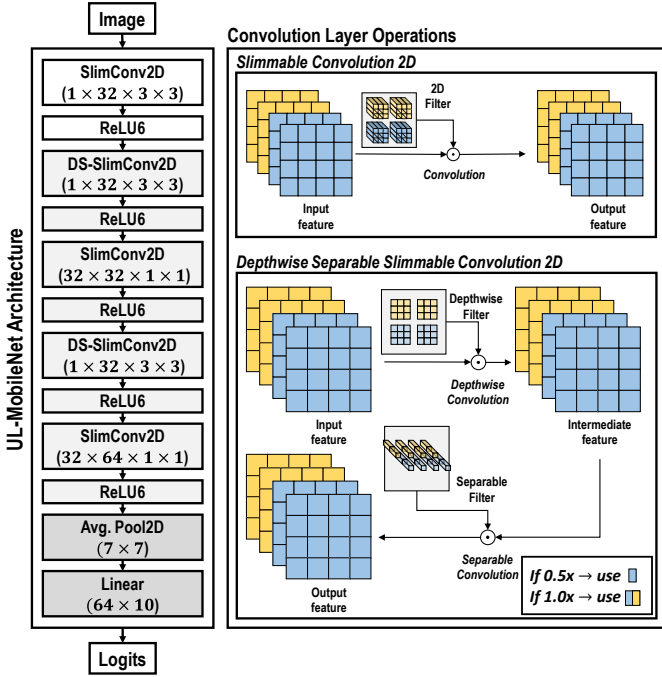


Fig. 2. Model architecture and its operation of UL-MobileNet. UL-MobileNet consists of 2-dimensional slimmable convolution layer (SlimConv2D), 2-dimensional depthwise separable slimmable convolution layer (DS-SlimConv2D), ReLU6 activation function, average pooling function (Avg. Pool2D) with 7×7 -sized kernel, and linear layer (Linear). SlimConv2D ($1 \times 32 \times 3 \times 3$) denotes that the kernel size is 3×3 , the number of input channels is 1, and the number of output channels is 32, respectively.

III. LOCAL MODEL ARCHITECTURE AND TRAINING

Currently, available SNN architectures and training algorithms are optimized for a standalone learning [13]. This section presents a novel SNN architecture for SlimFL, as well as its local training.

A. Ultra-Light MobileNet Architecture

This paper proposes *Ultra-Light MobileNet* (UL-MobileNet) under the consideration of the limited computing capacity of local. UL-MobileNet is presented in Fig. 2. UL-MobileNet consists of five convolution layers activated by ReLU6 function, average pooling function and linear layer. As shown in Fig. 2, two types of convolution layers exist. SlimConv2D and DS-SlimConv2D operate identically to a standard convolution layer and a depthwise separable convolutional layer, respectively. Both SlimConv2D and DS-SlimConv2D are width-adjustable convolutional layers. With adopting depthwise separable convolution (i.e., DS-SlimConv2D), the computing complexity is significantly reduced compared to standard convolution [29]. In our UL-MobileNet, we do not use BN, which is used in the state-of-the-art SNN architecture US-MobileNet proposed in [13]. As opposed to a *de facto* standard neural network architecture with a universal batch normalization layer, US-MobileNet is equipped with multiple separate BN layers to cope with all slimmable model configurations.

To describe the operation of the proposed UL-MobileNet, an input image (e.g., sneaker) and the ratio (e.g., 0.5x or 1.0x)

is given to UL-MobileNet. If the ratio is given 0.5x, half of the entire convolutional filter composing every layer (i.e., LH), is used as shown in Fig. 2. If the ratio is given 1.0x, the entire convolutional filter is used.

Hereafter, we consider that each device k has an SNN following the UL-MobileNet architecture. At the t -th iteration, the SNN model has the parameters θ_t^k with two width configurations: 0.5x width configuration $\theta_t^k \odot \Xi_1$ and 1.0x width configuration $\theta_t^k \odot \Xi_2 (= \theta_t^k)$, where \odot is the element-wise product and Ξ_i represents a binary mask for extracting the parameters of i -th width configuration.

B. Superposition SNN Training

Algorithm 1: SlimTrain [14]

- 1 Define *switchable width list* for slimmable network M , for example, $[0.25, 0.5, 0.75, 1.0] \times$.
 - 2 Initialize shared convolutions and fully-connected layers for slimmable network M .
 - 3 Initialize independent batch normalization parameters for each *width* in *switchable width list*.
 - 4 **for** $i = 1, \dots, n_{iters}$ **do**
 - 5 Get next mini-batch of data x and label y .
 - 6 Clear gradients of parameters, $optimizer.zero_grad()$.
 - 7 **for** *width* in *switchable width list* **do**
 - 8 Switch the batch normalization parameters of current width on network M .
 - 9 Execute sub-network M' at current width, $\hat{y} = M'(x)$.
 - 10 Compute loss, $loss = criterion(\hat{y}, y)$.
 - 11 Compute gradients, $loss.backward()$.
 - 12 **end**
 - 13 Update parameters, $optimizer.step()$.
 - 14 **end**
-

Training a multi-width SNN is arduous. The SNN back-propagation (BP) is warped due to gradient interference of multi-width. For example, the BP of 0.5x width configurations interferences the BP of 1.0x's and vice versa. This inter-width interference hinders not just inference accuracy but also training convergence. SlimTrain (see **Algorithm 1**), the first SNN training algorithm introduced in [14], partially ameliorates such inter-width interference by training alternative width configurations in descending order of size. While adhering to the sample principle, the authors of [13] have proposed a state-of-the-art SNN training technique called universal SNN (USTrain).

USTrain proposes the sandwich rule with the inplace knowledge distillation (IPKD), which are two notable techniques for training an SNN. To describe two notable techniques, the 1.0x model becomes a teacher guiding its sub-width models via knowledge distillation. By nature, it gives more benefits under a larger SNN (i.e., a better teacher) that has more sub-width configurations (i.e., more students). The IPKD encourages each sub-width (i.e., student) to provide a softmax output (i.e., logit) to that of the full-width (i.e., teacher), so that

Algorithm 2: USTrain [13]

```

1 Define width range, for example,
  [0.25, 0.5, 0.75, 1.0]x.
2 Define n as the number of sampled widths per training
  iteration, for example,  $n = 4$ .
3 Initialize training settings of shared network  $M$ .
4 for ( $t = 1, \dots, T_{iters}$ ) do
5   Get the next mini-batch of data  $x$  and label  $y$ ).
6   Clear gradients,  $optimizer.zero\_grad()$ .
7   Execute full-network,  $y' = M(x)$ .
8   Compute loss,  $loss = criterion(y', y)$ .
9   Accumulate gradients,  $loss.backward()$ .
10  Stop gradients of  $y'$  as label,  $y' = y'.detach()$ .
11  Add smallest width to width samples.
12  for width in width samples do
13    Execute sub-network at width,  $\hat{y} = M'(x)$ .
14    Compute loss,  $loss = criterion(\hat{y}, y')$ .
15    Accumulate gradients,  $loss.backward()$ .
16  end
17  Update parameters,  $optimizer.step()$ .
18 end

```

Algorithm 3: Superposition Training (SUSTRain)

```

1 Initialize train parameter
   $\Theta = \{\theta^1, \dots, \theta^k, \dots, \theta^K, \theta^G\}$ ,
2 Initialize local dataset  $\mathbf{Z} = \{Z_1, \dots, Z_k, \dots, Z_K\}$ 
  with Dirichlet distribution
3 Initialize learning rate  $\eta_t \leftarrow \eta_0$ 
4 Further Constraints:  $\hat{F}^1(\cdot) = F^1(\cdot) \triangleright$  Discuss in Sec. V
5 for  $t = 1, \dots, T$  do
6   for  $k = 1, \dots, K$  do
7     Initialize gradients of the model optimizer as 0.
8     Sample batch  $\zeta_t^k$  from  $Z_k$ .
9     Execute full-network  $M(\theta_t^k, \zeta_t^k)$ .
10    Compute loss,  $loss \leftarrow F^k(\theta_t^k, \zeta_t^k)$ .
11    Accumulate gradients,  $loss.backward()$ .
12    Execute full-network  $M(\theta_t^k, \zeta_t^k)$ .
13    Stop gradients of  $M(\theta_t^k, \zeta_t^k)$  as label.
14    for  $i = 1, \dots, S - 1$  do
15      Execute and calculate loss  $\hat{F}^k(\theta_t^k \odot \Xi_i, \zeta_t^k)$ 
16       $loss \leftarrow loss + w_i \hat{F}^k(\theta_t^k \odot \Xi_i, \zeta_t^k)$ .
17    end
18    Calculate gradient of  $loss$ .
19    Update model parameters.  $\triangleright$  Eq. (1)
20  end
21 end

```

their overlapping BP gradients become less dissimilar, hence minimizing the inter-width interference. At its core, the inplace distillation and the sandwich rule are effective under the case where an SNN can be divided into more than two segments. The SNN architecture considered in this paper consists of only the LH and RH segments, making the USTrain unfit for our case. Moreover, during updating the local parameters of slimmable model, some of the parameters composing small

model needs partial gradient calculation of big model.

While effective in standalone learning, in SlimFL with wireless connectivity, not all multi-width configurations are exchanged due to insufficient communication throughput. In other words, they exchanged width configurations are aggregated across devices, diluting the effectiveness of BN. In our experiments, we even observed training convergence failures due to BN. Furthermore, managing multiple BN layers not only consumes additional memory costs but also entails a high computing overhead.

To resolve this problem, we propose *superpositioned US-Train (SUSTRain)* algorithm. SUSTRain consists of two processes. First, all the forward propagation losses (FP) are holden. Then, all the width configurations are concurrently updated with the superpositioned gradients. With SUSTRain, a sub-width configuration (i.e., student) is trained using IPKD without the logit mismatch with its full-width configuration's logit (i.e., teacher's logit), while the full-width configuration is simultaneously trained using the ground truth.

In this paper, we consider that all devices have SNN with two-width configurations (i.e., one teacher and one student). Hereafter, we generalize the local SNN update rule for the device k described as follows:

$$\theta_{t+1}^k = \theta_t^k - \eta_t [w_1 \nabla \hat{F}^k(\theta_t^k \odot \Xi_1, \zeta_t^k) + w_2 \nabla F^k(\theta_t^k \odot \Xi_2, \zeta_t^k)], \quad (1)$$

where $w_1 + w_2 = 1$ and $w_1, w_2 > 0$. The operator \odot implies element-wise multiplication for extracting the parameters which is allocated to the SNN width configuration. The term $\eta_t > 0$ is a learning rate, and ζ_t^k implies a stochastic input realization. The function $F^k(\theta_t^k \odot \Xi_i, \zeta_t^k)$ is the cross-entropy between the ground truth $y(\zeta_t^k)$, whereas the IPKD function $\hat{F}^k(\theta_t^k \odot \Xi_i, \zeta_t^k)$ is the cross-entropy between the logit $M(\theta_t^k, \zeta_t^k)$ of the full-width configuration and the logit $M(\theta_t^k \odot \Xi_i, \zeta_t^k)$ of the i -th width configuration. The details of SUSTRain are in **Algorithm 3**.

IV. GLOBAL MODEL AGGREGATION WITH SUPERPOSITION CODING & SUCCESSIVE DECODING

A. Superposition Coding & Successive Decoding

1) *Wireless Systems*: This paper considers a frequency division duplex (FDD) environment in this paper [30]. FDD allows the server and devices to perform uplink and downlink transmissions simultaneously, without any interference between the uplink and downlink signals. In addition, we consider a wireless communication system with an orthogonal scheme such as an orthogonal frequency-division multiple access (OFDMA), time division multiple access (TDMA), or code division multiple access (CDMA) [30]. With an orthogonal scheme, the inter-device interference is negligible. Additionally, we assume that the server has sufficient bandwidth resources and that each device is assigned a fixed amount of bandwidth. As a result, the total bandwidth is proportional to the device count.

2) *Decoding Success Probability*: The successful reception of a wireless signal is mainly affected by the signal-to-

interference-plus-noise ratio (SINR) [26]. At a receiver, SINR is given as follows:

$$\gamma = \chi d^{-\beta} P / (\sigma^2 + P^I), \quad (2)$$

where P , P^I , and σ^2 denote the transmit, receive interference, and noise powers, respectively. Additionally, d is a transmitter-receiver distance, $\beta \geq 2$ is a path loss exponent, and χ is small scale fading (i.e., Rayleigh fading). Following the Shannon's capacity formula with a Gaussian codebook, the received throughput R with the bandwidth W is $R = W \log_2(1 + \gamma)$ (bits/sec). When the transmitter encodes raw data with a code rate u , its receiver successfully decodes the encoded data if $R > u$. The decoding success probability is,

$$\Pr(R \geq u) = \Pr\left(\frac{\chi d^{-\beta} P}{\sigma^2 + P^I} \geq u'\right). \quad (3)$$

where $u' = 2^{\frac{u}{W}} - 1$. The decoding success probability with SC and SD is given by balancing P and P^I as elaborated next.

3) *Superposition Coding (SC)*: We focus on transmitting S messages from a transmitter to a receiver at the same time. Before transmission, these messages are SC-encoded [8], and the whole transmission power budget P is allotted to the i -th message, with $P = \sum_{i=1}^S P_i$ transmission power for $i \in [1, S]$. There is no interference on reception when just a single message is sent, i.e. $S = 1$ and $P^I = 0$. The interference for $S > 1$ is determined by SD as elaborated next.

4) *Successive Decoding (SD)*: The SC-encoded message is meant to be sequentially decoded at the receiver by first decoding the strongest signal, then canceling out the decoded signal, and finally decoding the next strongest signal, i.e., SD, also known as successive interference cancellation [31]. The small-scale fading parameter χ under Rayleigh fading follows an exponential distribution, i.e., $\chi \sim \text{Exp}(1)$. Assuming $P_i > P_{i'}$ and $i' > i$, the receiver may gradually decode the i -th message while experiencing the remaining the messages as its interference P_i^I , i.e., $P_i^I = \chi d^{-\beta} \hat{P}_i^I$, where $\hat{P}_i^I \triangleq \sum_{i'=i+1}^S P_{i'}$ for $i \leq S - 1$, and $\hat{P}_S^I = P_S^I = 0$ as there is no interference for the last message. Assume that R_i represents the throughput of the i -th message. By substituting P_i^I into (3), we get the distribution of R_i as $\Pr(R_i \geq u) = \Pr\left(\chi \geq \frac{c}{P_i/u' - \hat{P}_i^I}\right)$, where $c = \sigma^2 d^\beta$. By using this result, i -th message's decoding success probability p_i is as follows:

$$p_i = \Pr(R_1 \geq u, R_2 \geq u, \dots, R_i \geq u) \quad (4)$$

$$= \Pr\left(\chi \geq \frac{c}{P_1/u' - \hat{P}_1^I}, \dots, \chi \geq \frac{c}{P_i/u' - \hat{P}_i^I}\right) \quad (5)$$

$$= \Pr\left(\chi \geq \max\left\{\frac{c}{P_1/u' - \hat{P}_1^I}, \dots, \frac{c}{P_i/u' - \hat{P}_i^I}\right\}\right). \quad (6)$$

B. SlimFL Operations

We discuss SlimFL and global model aggregation in further detail. SlimFL is denoted by the symbols shown in Table I. **Algorithm 4** describes the fundamental SlimFL operations.

Algorithm 4: SlimFL with SC & SD

```

1 Initialize train parameters
   $\Theta = \{\theta^1, \dots, \theta^k, \dots, \theta^K, \theta^G\}$ .
2 Split dataset  $\mathbf{Z}$  into  $K$  datasets
   $\mathbf{Z} = \{Z_1, \dots, Z_k, \dots, Z_K\}$ .
3 while Training do
4   //Local Model Training (Algorithm 1)
5   for  $k = 1, \dots, K$  do
6     for  $\zeta_k$  in  $Z_k$  do
7       | Update local model parameter  $\theta^k \triangleright$  Eq. (1)
8     end
9   end
10  //SC&SD-based Server Aggregation (Uplink)
11  if Aggregation Period then
12     $n_L = |\text{HUF}| \leftarrow 0, n_R = |\text{F}| \leftarrow 0,$ 
13     $\text{H} \leftarrow \emptyset, \text{F} \leftarrow \emptyset$ 
14    for  $k = 1, \dots, K$  do
15       $g \leftarrow \text{rand}(1)$ 
16      if  $p_2 \leq g < p_1$  then
17        |  $\text{H} \leftarrow \text{H} \cup k, n_L \leftarrow n_L + 1$ 
18      end
19      if  $g \geq p_2$  then
20        |  $\text{F} \leftarrow \text{F} \cup k, n_L \leftarrow n_L + 1, n_R \leftarrow n_R + 1$ 
21      end
22    end
23     $\triangleright$  Case1.  $n_L > 0, n_R > 0$ 
24     $\theta^G \leftarrow$ 
25     $\frac{1}{|\text{HUF}|} \sum_{k \in \text{HUF}} \theta^k \odot \Xi + \frac{1}{|\text{F}|} \sum_{k \in \text{F}} \theta^k \odot \Xi^{-1}$ 
26     $\triangleright$  Case2.  $n_L > 0, n_R = 0$ 
27     $\theta^G \leftarrow \frac{1}{n_L} \sum_{k \in \text{H}} (\theta^k \odot \Xi)$ 
28     $\triangleright$  Case3.  $n_L = n_R = 0$ 
29    Skip aggregation
30  end
31  //Local Update (Downlink)
32  for  $n = 1, \dots, K$  do
33    |  $\theta^k \leftarrow \theta^G$ 
34  end

```

The network consists of K devices that are linked through wireless connections to a parameter server. Each device uses SC whilst communicating with the server, whereas the server uses SD. To be more descriptive, k -th device has a local dataset $Z^k \in \mathbf{Z}$ and an SNN parameter θ^k with two width configurations. Across devices, the global data \mathbf{Z} may be IID or non-IID. Each SNN θ^k is subdivided into an LH $\theta^k \odot \Xi$ and a RH segment $\theta^k \odot \Xi^{-1}$, where $\Xi = \Xi_1$ and $\Xi^{-1} = \Xi_2 - \Xi_1$. Superposition training is used to train the k -th local device (lines 4–9), which is expressed as (1). The local device transmits to the server the SC-encoded local model θ^k . Each local device transmits two messages (i.e., LH and RH segments), each with a distinct transmission power P_1 and P_2 relative to $P_1 \gg P_2$. In accordance with (6), after reception, the server can successively decode using SD and

obtain: (i) a 0.5x model if $\chi \geq c/(P_1/u' - P_2)$ (lines 15–17) is satisfied; (ii) 1.0x model if the channel fading gain satisfies $\chi \geq \max\{c/(P_1/u' - P_2), c/(P_2/u')\}$ (lines 18–20); and (iii) otherwise it obtains no model. As a result, the RH segments from F of devices and the LH segments from $H \cup F$ of devices are combined by the server.

V. SLIMFL CONVERGENCE ANALYSIS

A. Assumptions

In order to analyze the convergence rate of SlimFL, following assumptions are considered.

- 1) Regardless of SC or SD, downlink decoding is always successful (**Algorithm 4**, lines 29–32). The fact that the server (e.g., a base station) has a far higher broadcast power than the uplink power contributes to this.
- 2) We assume that K is big enough that $|H \cup F| \approx Kp_1$ and $|F| \approx Kp_2$, where p_1 and p_2 are the LH and RH segment decoding success probability, respectively, provided in (6). As a result, during the t -th communication cycle, the server builds the following global model θ_t^G :

$$\theta_t^G \leftarrow \frac{1}{Kp_1} \sum_{k \in H \cup F} \theta_t^k \odot \Xi + \frac{1}{Kp_2} \sum_{k \in F} \theta_t^k \odot \Xi^{-1}. \quad (7)$$

- 3) One communication round is assumed per local iteration or mathematically tractability. According to [32], FedAvg does not guarantee that a number of local iterations is proportional to the performance. Since the number of local iterations at each communication round is 1, superscript G is omitted, resulting in $\theta_t = \theta_t^G$. This assumption will be further discussed in Sec VI-D3.

Based on these assumptions, the convergence analysis of SlimFL is mathematically tractable as discussed in Sec. V-B.

B. Convergence Analysis

This paper analyzes the convergence of SlimFL in non-IID data distribution. We follow the fundamental derivation techniques utilized [22], [24] for FedAvg. One significant challenge in the convergence analysis for SlimFL is due to the local model updates in (1) and the global model aggregation in (7) include sophisticated binary masks owing to the SNN architecture as well as SC and SD. As a result, unlike FedAvg, whose global objective function is the weighted average of local loss functions $\{F^k(\theta_t^k)\}$, i.e., empirical risk, SlimFL's objective function $F(\theta_t)$ is unknown. Alternatively, we define $F(\theta_t)$ in terms of its gradient $f_t = \nabla F(\theta_t)$, which can be obtained using SlimFL's local and global operations, as discussed below. After a downlink, the device k replaces its local model with the downloaded global model, represented by $\theta_t^k \leftarrow \theta_t$. The device then changes the local model in the following:

$$\theta_{t+1}^k \leftarrow \theta_t - \eta_t g_t^k, \quad (8)$$

where $g_t^k = \sum_{i=1}^2 w_i \nabla F^k(\theta_t \odot \Xi_i, \zeta_t^k)$ follows from (1). We assume that the student's soft goal may be approximated by the student's hard objective, i.e.,

$$\hat{F}^k(\theta_t \odot \Xi_i, \zeta_t^k) \approx F^k(\theta_t \odot \Xi_i, \zeta_t^k). \quad (9)$$

Next, after the uplink, the server aggregates the updated local models to form the global model θ_{t+1} . By applying (8) to (7), the resulting global model is as follows:

$$\begin{aligned} \theta_{t+1} &= \frac{1}{Kp_1} \sum_{k \in H \cup F} (\theta_t - \eta_t g_t^k) \odot \Xi + \frac{1}{Kp_2} \sum_{k \in F} (\theta_t - \eta_t g_t^k) \odot \Xi^{-1} \\ &= \theta_t - \eta_t \underbrace{\left(\frac{1}{Kp_1} \sum_{k \in H \cup F} g_t^k \odot \Xi + \frac{1}{Kp_2} \sum_{k \in F} g_t^k \odot \Xi^{-1} \right)}_{:=f_t}, \end{aligned} \quad (10)$$

resulting in f_t in (10), which characterizes $F(\theta_t)$. In (10), the last step can be obtained from $|H \cup F| = Kp_1$, $|F| = Kp_2$, and $\theta_t = \theta_t \odot (\Xi + \Xi^{-1})$.

Hereafter we use the bar notation $\bar{\cdot}$ for the value averaged over $\{\zeta_t^k\}$, and $*$ for indicating the optimum. For the functions F and $\{F^k\}$, we analyze the following commonly used assumptions in the literature [24], [33].

Assumption 1. (L-smoothness) F and $\{F^k\}$ are L -smooth, i.e.,

$$F^k(\theta_v) \leq F^k(\theta_w) + (\theta_v - \theta_w)^T \nabla F^k(\theta_w) + \frac{L}{2} \|\theta_v - \theta_w\|^2 \quad (11)$$

for all $v, w > 0$.

Assumption 2. (μ -strong convexity) F and $\{F^k\}$ are μ -strong convex: i.e.,

$$F^k(\theta_v) \geq F^k(\theta_w) + (\theta_v - \theta_w)^T \nabla F^k(\theta_w) + \frac{\mu}{2} \|\theta_v - \theta_w\|^2 \quad (12)$$

for all $v, w > 0$.

Since linear sum preserves strong convexity and smoothness, \bar{F}^k also has the μ -strong convexity and L -smoothness. In addition, we also assume our global model has same properties.

Assumption 3. (Bounded local gradient variance) The variance of the local gradient $\nabla F^k(\theta^k, \zeta_t^k)$ is bounded within Z_k , which is given as

$$\mathbb{E}[\|\nabla F^k(\theta^k, \zeta_t^k) - \nabla \bar{F}^k(\theta)\|^2] \leq \sigma_k^2. \quad (13)$$

Inspired by [22], we define a factor that measures the non-IIDness of Z as:

$$\delta = \frac{1}{K} \sum_{k=1}^K \sigma_k^2. \quad (14)$$

Indeed, the variance (over k) of the local gradient variance (over Z_k) is defined as:

$$\bar{\sigma} \triangleq \frac{1}{K} \sum_{k=1}^K \left(\sigma_k - \frac{1}{K} \sum_{k=1}^K \sigma_k \right)^2. \quad (15)$$

This characterizes the data distributions over devices, and so does δ without loss of generality.

To prove the convergence of SlimFL, we derive the following two lemmas as referred to Appendix A-A, A-B.

Lemma 1. (Bounded global gradient variance) Under Assumption 3, the variance of the global gradient f_t is bounded

within \mathbf{Z} , which is given as

$$\mathbb{E}\|f_t - \bar{f}_t\|^2 \leq B \quad (16)$$

where $B = 4\delta(\frac{1}{p_1} + \frac{1}{p_2}) \sum_{i=1}^2 w_i^2$.

Lemma 2. (Per-round global model progress) Under Assumptions 1 and 2 with a learning rate $\eta_t \leq \frac{1}{L}$, the error between the updated global model and its optimum progress as

$$\mathbb{E}\|\theta_{t+1} - \theta^*\|^2 \leq (1 - \frac{\mu\eta_t}{2})\mathbb{E}\|\theta_t - \theta^*\|^2 + \eta_t^2 B. \quad (17)$$

By Lemma 1 and Lemma 2, the convergence of SlimFL is proved. The full derivation of this proof is in Appendix A-C.

Theorem 1. (SlimFL Convergence) Under Assumptions 1–3 with the learning rate $\eta_t = \frac{2}{\mu t + 2L - \mu}$, one has

$$\mathbb{E}[F(\theta_t)] - F^* \leq \frac{L}{\mu} \cdot \frac{\mu L \Delta_1 + 2B}{\mu t + 2L - \mu}, \quad (18)$$

where $B = 4\delta(\frac{1}{p_1} + \frac{1}{p_2}) \sum_{i=1}^2 w_i^2$ and $\Delta_t \triangleq \mathbb{E}\|\theta_t - \theta^*\|^2$. Therefore, $\mathbb{E}[F(\theta_t)]$ converges to F^* as $t \rightarrow \infty$.

The result of Theorem 1 exhibits several insights of SlimFL as follows.

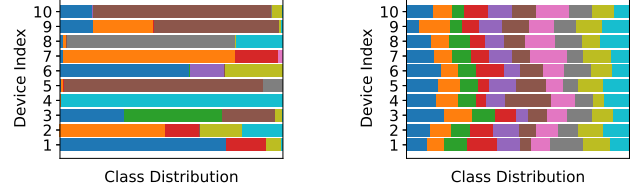
1) *Failure under extremely poor channels:* Consider a channel with very poor quality, where the server is unable to decode 1.0x models and hence collects only 0.5x models (i.e., $p_2 \approx 0$ and $p_1 > 0$). In this case, despite the fact that the optimality gap aggregates 0.5x models, it diverges. In these channel conditions, SC becomes inefficient, and vanilla FL with 0.5x models is preferred to SlimFL.

2) *Robustness to poor channels:* In (18), we confirm that increasing the number of 0.5x and 1.0x models aggregated (i.e., increasing p_1 and p_2) helps equally to close the global optimal bound. As a result, aggregating 0.5x models can further alleviate 1.0x models' frequent decoding failures on poor channels.

3) *Robustness to non-IID data:* The optimality gap widening as δ (i.e., more non-IID). Contrary to vanilla FL, which benefits primarily from aggregating either 0.5x or 1.0x models, SlimFL's increased gap may be mitigated by aggregating not just 1.0x but also 0.5x models. Hence, we conclude that SlimFL is superior for non-IID data distributions and moderately poor channel conditions where $0 \ll p_1, p_2 < 1$. Vanilla FL with just 1.0x models or 0.5x models is recommended for highly excellent (i.e., $p_2 \approx 1$) or extremely bad (i.e., $p_1 \approx 0$) channel conditions, respectively. SlimFL's favorable conditions and efficacy will be validated by simulation in Sec. VI. Additionally, as detailed in the following two propositions, Theorem 1 gives design principles for SC and ST.

Proposition 1 (Optimal SC power allocations). Consider the SC power allocation ratio $\lambda \in (0.5, 1]$ such that $P_1 = \lambda P$ and $P_2 = (1 - \lambda)P$. If $\lambda \gg \max\{0.5, cu'(1 + u')/P\}$, the optimal SC power allocation ratio that minimizes the RHS of (18) is given as

$$\lambda^* = \frac{u' + \sqrt{1 + u'} - 1}{u'}. \quad (19)$$



(a) Non-IID ($\alpha = 0.1$).

(b) IID ($\alpha = 10$).

Fig. 3. An illustration of the data distributions across 10 devices for the different values of the Dirichlet concentration ratio α . Note that each color represents each class constituting the dataset.

Proof. Define $D \triangleq \frac{1}{p_1} + \frac{1}{p_2}$. According to the RHS of (18), λ^* minimize D . Since $P_1 > P_2$, we have

$$D = \exp\left(-\frac{c}{\lambda P/u' - (1 - \lambda)P}\right) + \exp\left(-\frac{c}{(1 - \lambda)P/u'}\right). \quad (20)$$

If $\lambda \gg cu'(1 + u')/P$, we can approximate both terms in D using the first-order Taylor expansion, yielding

$$D \approx 2 + \frac{c}{\lambda P/u' - (1 - \lambda)P} + \frac{c}{(1 - \lambda)P/u'}. \quad (21)$$

The approximated D is convex, and the first-order necessary condition gives the optimum. \square

Note that the condition $\lambda \gg \max\{0.5, cu'(1 + u')/P\}$ can be satisfied under sufficiently small model sizes (e.g., $t' \rightarrow 0$), wide bandwidth (e.g., $W \rightarrow \infty$), good channel conditions (e.g., $\sigma^2 \rightarrow 0$), and/or a large total transmit power budget (e.g., $P \rightarrow \infty$).

Proposition 2 (Optimal ST ratio). The optimal ST ratio that minimize the RHS of (18) are given as $w_1^* = w_2^* = 1/2$.

Proof. The RHS of (18) is minimized at the minimum of $\sum_{i=1}^2 w_i^2$. By the C-S inequality, we have

$$\sum_{i=1}^2 w_i^2 \geq \frac{1}{2} \left(\sum_{i=1}^2 w_i \right)^2. \quad (22)$$

The desirable result is obtained by combining the condition $\sum_{i=1}^2 w_i = 1$ in (1) with the equality condition of the AM-GM inequality. The influence of λ^* and w_i^* will be demonstrated by simulation in the next section. \square

VI. EXPERIMENTS

We investigate the effectiveness and feasibility of SlimFL corresponding to the numerical results of convergence analysis, the robustness to various channel conditions and non-IID data distributions, and computation/communication efficiency.

A. Simulation Settings

To show the effectiveness of the proposed SlimFL, we consider a classification task with the Fashion MNIST (FMNIST) image dataset [34]. The impact of other datasets such as the CIFAR-10 and MNIST datasets will be discussed in VI-D. The dataset is randomly sharded and distributed across devices.

TABLE II
SIMULATION PARAMETERS.

Description	Value
Initial learning rate (η_0)	10^{-3}
Optimizer	Adam
Batch size	64
Distance (d)	100 [m]
Path loss exponent (β)	2.5
Bandwidth per device (W)	75 [MHz]
Uplink transmission power (P)	23 [dBm]
Central frequency	5.9 [GHz]
Noise power spectrum	-169 [dB/Hz]

Following [35], the non-IIDness of the data distribution is modeled using a Dirichlet distribution with its concentration parameter $\alpha \in \{0.1, 1.0, 10\}$, where the higher α implies the more non-IID data distribution as illustrated in Fig 3. We consider a single communication round consisting of a pair of uplink and downlink transmissions for each local training iteration. The communication channels over different devices are orthogonal in both uplink and downlink. The Rayleigh fading gain χ for each channel realization follows an exponential distribution $\chi \sim \text{Exp}(1)$ [26]. The corresponding communication and neural network hyperparameters are summarized in Table II. We adopt Vanilla FL as a comparison technique. Vanilla FL is widely used FL technique (i.e., FedAvg) with fixed-width SNN model without leveraging SC nor SD. We consider three Vanilla FL schemes as listed follows:

- 1) *Vanilla-FL 0.5x/1.0x*: Vanilla FL 0.5x and 1.0x use only 0.5x- or 1.0x-width configurations, respectively. We compare model accuracy and the convergence of SlimFL with Vanilla FL-0.5x and 1.0x corresponding to the robustness to various channel conditions and non-IIDness in Sec. VI-B.
- 2) *Vanilla-FL 1.5x*: Due to the lack of width-adjustable SNNs, each device in Vanilla FL-1.5x separately runs fixed-width 0.5x and 1.0x models. Then, devices can choose the 0.5x or 1.0x model considering energy heterogeneity, which SlimFL can. In other words, Vanilla FL-1.5x operates the two FedAvg operations separately for 0.5x and 1.0x models by doubling the bandwidth, transmission power, and computing resources. By comparing SlimFL to Vanilla FL-1.5x, we investigate the difference of accuracy, received bits and energy cost.

B. Efficiency, Robustness, and Scalability of SlimFL

We carry out to analyze SlimFL’s performance to Vanilla FL in situations with a variety of communication conditions and non-IID settings. To assess the efficiency of communication and computation, we first calculate computation cost for UL-MobileNet feed-forwarding [36] and communication cost per one communication round.

- 1) *Communication Efficiency*: Between ten devices and a server, the total quantity of data communicated is 205.8MBytes for SlimFL and Vanilla FL-1.0x, and

TABLE III
COMPUTING COSTS AND TRANSMISSION POWER OF UL-MOBILENET.

Description		1.0x	0.5x
Computation	MFLOPS / round	2.76	0.79
	# of parameters	4, 586	2, 293
	Bits / round	172, 688	86, 344
Transmission Power (P) [mW]		132.1	67.4

TABLE IV
TRANSMISSION AND COMPUTING COSTS PER COMMUNICATION ROUND.

Metric	SlimFL	Vanilla FL-1.5x
Communication Cost [mW/Round]	199.5	399.1
Computation Cost [MFLOPS/Epoch]	3.56	3.56

TABLE V
SUCCESSFULLY DECODED BITS OF SLIMFL, AND VANILLA FL.

FL Scheme	Decoding	Channel Condition	
		Good	Poor
SlimFL	0.5x	1.96	18.32
	1.0x	198.45	130.10
	None	5.46	57.44
Vanilla FL-0.5x	0.5x	102.21	93.87
	None	0.72	9.06
Vanilla FL-1.0x	1.0x	200.30	144.93
	None	5.56	60.96

TABLE VI
TOTAL COMPUTATION COST AND TRANSMISSION POWER OF SLIMFL AND VANILLA FL-1.5x IN VARIOUS NON-IIDNESS ($\alpha = 0.1, 1.0, 10$).

Metric	non-IIDness	SlimFL		Vanilla FL-1.5x	
		Good	Poor	Good	Poor
Communication Cost [W]	$\alpha = 0.1$	71.0	57.3	158.8	196.8
	$\alpha = 1.0$	8.5	10.4	15.8	36.7
	$\alpha = 10$	3.03	3.51	10.2	25.4
Computation Cost [GFLOPS]	$\alpha = 0.1$	1.27	1.02	1.88	2.41
	$\alpha = 1.0$	0.15	0.18	0.22	0.51
	$\alpha = 10$	0.05	0.06	0.14	0.35

102.9MBytes for Vanilla FL-0.5x under ideal channel conditions (i.e., always successful decoding). We investigate the efficiency of communication resources in both good and bad channel conditions to validate the effectiveness of SC and SD. The experimental result for this subsection is presented in Table V, which shows that SlimFL delivers up to 3.52% fewer dropped bits than Vanilla FL-1.0x when SC and SD are being used. SlimFL enjoys the benefits mentioned above while consuming only half of the transmission power and bandwidth compared to Vanilla FL-1.5x, as presented in Table V, corroborating its communication efficiency. Because a part of the transmission power of SlimFL is allocated to 0.5x models, SlimFL decodes less than 1.0x model bits than Vanilla FL-1.0x. In return, SlimFL receives not only 1.0x models but also 0.5x models simultaneously. The additional

TABLE VII
ACCURACY UNDER DIFFERENT CHANNEL CONDITIONS AND α .

Method	Top-1 Accuracy (%)					
	Good		Poor			
	$\alpha = 0.1$	$\alpha = 1$	$\alpha = 10$	$\alpha = 0.1$	$\alpha = 1$	$\alpha = 10$
SlimFL-0.5x	54 ± 2.2	83 ± 1.0	85 ± 1.0	56 ± 2.4	82 ± 1.7	85 ± 1.1
SlimFL-1.0x	59 ± 2.3	85 ± 1.1	87 ± 1.1	65 ± 2.9	84 ± 1.4	87 ± 0.9
Vanilla FL-0.5x	45 ± 5.9	84 ± 1.1	85 ± 1.0	39 ± 8.3	83 ± 1.2	85 ± 0.9
Vanilla FL-1.0x	69 ± 5.8	85 ± 4.0	86 ± 4.3	55 ± 9.2	80 ± 6.0	82 ± 4.7

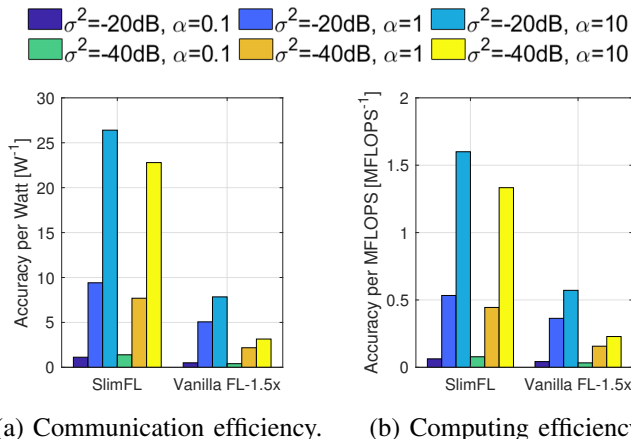


Fig. 4. Energy efficiency comparison between SlimFL and Vanilla FL-1.5x, in terms of (a) accuracy per unit communication energy and (b) accuracy per accuracy per unit computing energy.

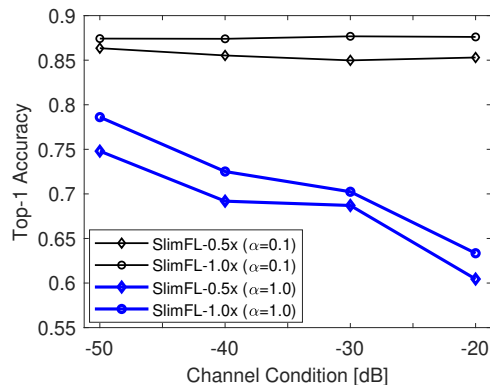


Fig. 5. Test accuracy in various channel conditions (e.g., -50dB, -40dB, -30dB and -20dB) with various non-IIDness (e.g., $\alpha = 0.1$ and $\alpha = 10$).

received 0.5x models coincide with the LH parts of the 1.0x models, which improve the accuracy and convergence speed of both 0.5x and 1.0x models.

2) *Energy Efficiency*: Thus far, we have evaluated SlimFL’s performance after training using 1,000 epochs. We estimate the energy consumption till convergence in this section. Numerical convergence in training is defined as the point at which the standard deviation (std) of test accuracy falls below a predefined threshold and the lowest test accuracy exceeds the average test accuracy in 100 consecutive rounds. To assess model convergence, we establish the reference values for the mean μ_{Ref} as 80% and σ_{Ref} as 7.25%, respectively.

Convergence occurs when the average Top-1 accuracy for 100 consecutive epochs is greater than μ_{Ref} and the average std is less than σ_{Ref} . With this convergence criterion, Table VI compares the overall energy costs of SlimFL and Vanilla FL-1.5x until convergence, based on the communication and processing energy costs per round in Table IV. As shown in Table VI, harsh non-IIDness ($\alpha = 0.1$) with poor channel conditions makes FL convergence hard. SlimFL, on average, produces a 3.6x reduction in total computing costs and a 2.9x reduction in total communication costs until their convergences. In addition, Fig. 4 shows the energy efficiency results corresponding to accuracy. As shown in Fig. 4(a), SlimFL requires only the 32.63% of Vanilla FL-1.5x’s total communication cost for model convergence. Similarly, the computing cost for SlimFL is the 44.37% of Vanilla FL-1.5x’s as shown in Fig. 4(b). This increased energy efficiency is according to SlimFL’s faster convergence even in non-IID and/or bad channel circumstances caused by SC and SD.

3) *Robustness to Poor Channels*: SlimFL and Vanilla FL both achieve high accuracy when channel conditions are good, as shown in Fig. 6 and Table VII. When the channel condition deteriorates from good to poor, however, as shown in Fig. 6(c,f) and Table VII, Vanilla FL1.0x’s maximum accuracy at $\alpha = 10$ declines from 86 to 82 percent. SlimFL-1.0x, on the other hand, retains its maximum accuracy of 87 percent at $\alpha = 10$ in both good and bad channel conditions. Additionally, at $\alpha = 0.1$, SlimFL-1.0x outperforms Vanilla FL-1.0x by 18% in terms of top-1 accuracy, despite the fact that Vanilla FL-1.0x consumes more communication and computing resources. Additionally, as the channel condition degrades, the std of Vanilla FL-1.0x’s top-1 accuracy increases by up to 59%, while SlimFL’s std increases by just 31%. These findings show SlimFL’s resistance to poor channels conditions, as well as its resistance to non-IID data distributions (low α) and communication efficiency.

4) *Robustness to Non-IID Data*: SlimFL-0.5x has a stable convergence under $\alpha = 0.1$ condition, as indicated in Fig. 6(d-f) and Table VII. In poor channel conditions and with the non-IID distribution ($\alpha = 0.1$), Vanilla FL-0.5x and Vanilla FL-1.0x display the std of 8.3 and 9.2. On the other hand, SlimFL-0.5x and SlimFL-1.0x both demonstrate the std of 2.4 and 2.9 with top-1 accuracy. This propensity persists even when $\alpha = 1$, $\alpha = 10$ are prevalent. SlimFL-1.0x and SlimFL-0.5x have a smaller coefficient of variation than Vanilla FL-1.0x and Vanilla FL-0.5x. This accentuates SlimFL’s robustness to non-IID data on poor channels.

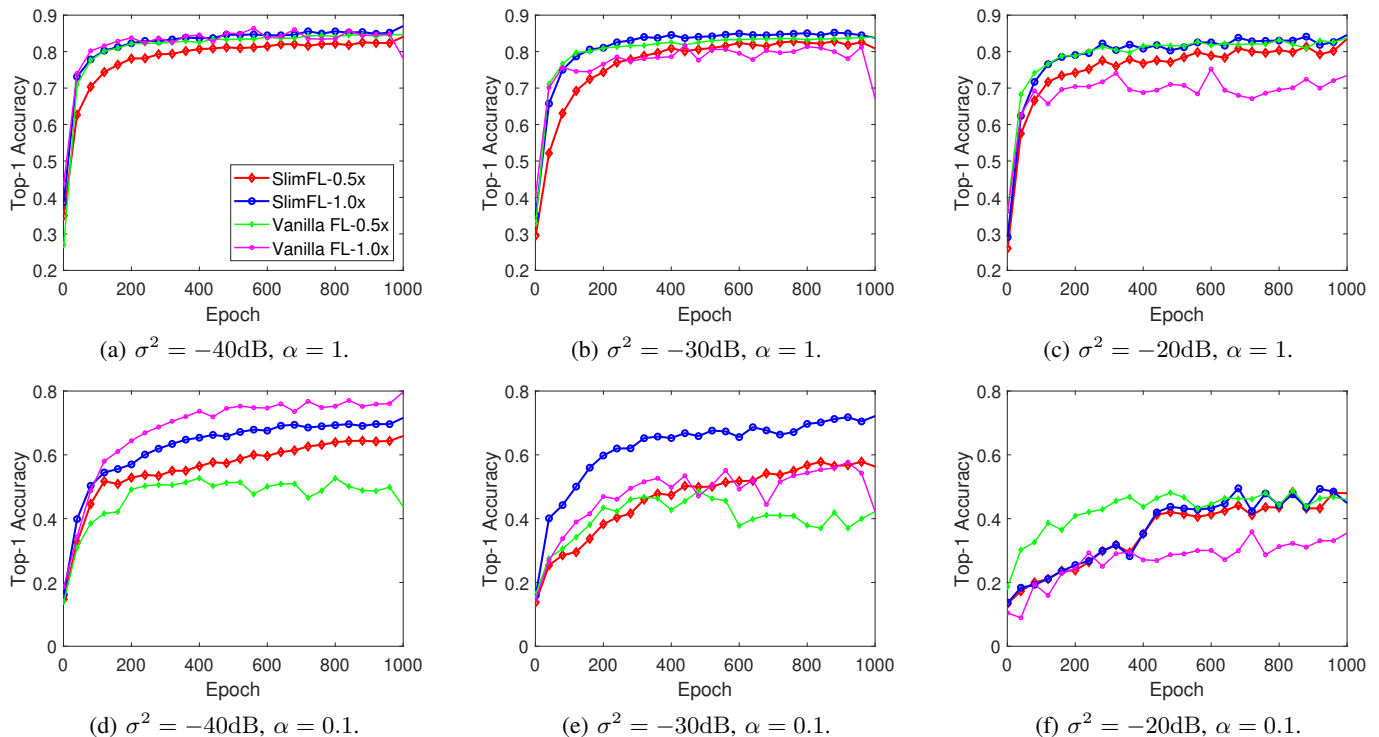


Fig. 6. Test accuracy in various channel noise conditions (on average). (a-c) are with $\alpha = 1$, (d-f) are with $\alpha = 0.1$.

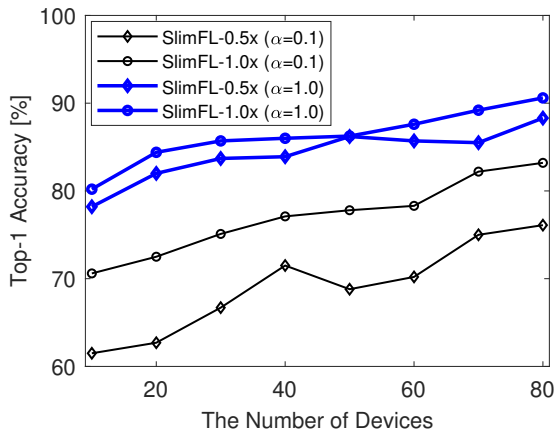


Fig. 7. Top-1 accuracy with the different number of devices.

5) *Scalability*: As shown in Fig. 7, SlimFL’s accuracy increases as the number of federating devices increases. The SlimFL-0.5x achieves an accuracy of up to 79%, while the SlimFL-1.0x reaches an accuracy of up to 85%. Additionally, with non-IIDness ($\alpha = 0.1$) and 70 federating local devices, SlimFL-0.5x achieves a greater level of accuracy than SlimFL-1.0x with 20 federating local devices. Based on the experimental results, it is expected that when constructing a FL system using non-IID datasets, optimality can be obtained by adjusting the number of local devices and width through SlimFL adaption.

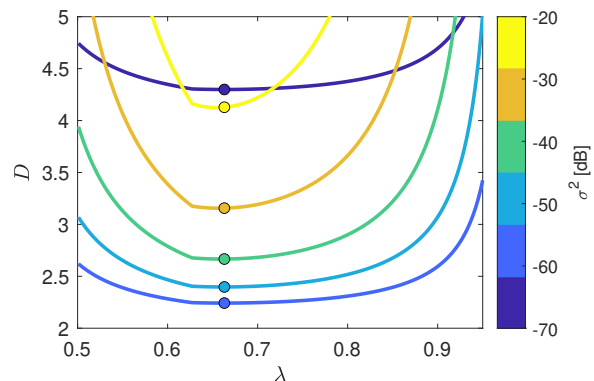


Fig. 8. SC power allocation ratio λ versus D ($= p_1^{-1} + p_2^{-1}$).

C. Ablation Studies on Optimization and Local Training

1) Effectiveness of SC Power Allocation Optimization:

We present a method for optimizing our suggested model by modifying the ST parameter w_i . The numerical results of optimal λ^* are shown in Fig. 8. The derivative of the Taylor expansion is used in Proposition 1 to compute λ^* . The ideal power allocation factor is $\lambda^* = 0.662$, which is the same value as the numerical optimum, as determined by the analytical solution. The simulation was carried out using the baseline with $\lambda = 0.8$ in a non-IID settings (i.e., $\alpha = 0.1$) to verify the recommendation from Proposition 1. The experiment’s result is shown in Fig. 9(a). The top-1 accuracy with λ^* is 6.4% higher than top-1 accuracy with 0.5x and 8.8% higher than top-1 accuracy with 1.0x. To put it another way, Proposition 1 acts as a guiding principle in SlimFL.

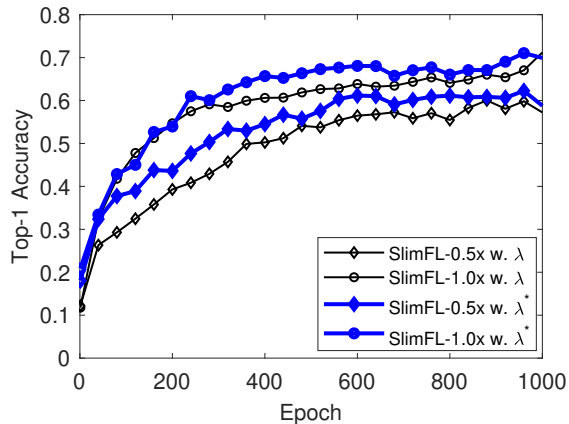
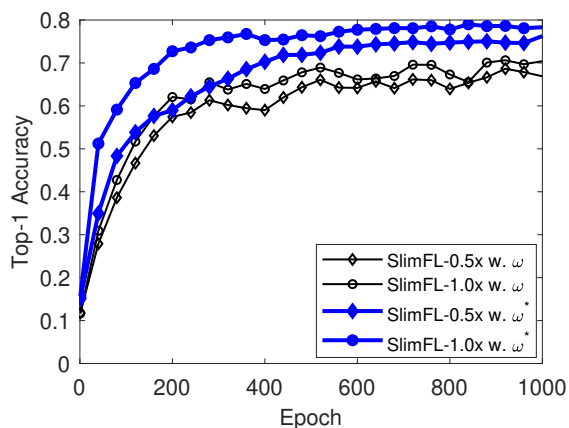
(a) SC power allocation ratio (λ).(b) ST ratio (w_i)

Fig. 9. Top-1 accuracy under optimal and non-optimal design parameters: (a) $\lambda^* = 0.663$ and $\lambda = 0.8$, and (b) $w_1^* = w_2^* = 0.5$ and $(w_1 = 0.3, w_2 = 0.7)$ with $\alpha = 0.1$.

2) *Effectiveness of ST Ratio Optimization:* When $w_1 = \dots = w_S = \frac{1}{S}$ in Proposition 2, SlimFL has a tight bound. Since $S = 2$ is taken into account in our proposed scheme, all hyperparameters that make up ST should be 0.5, i.e., $(w_1^*, w_2^*) = (0.5, 0.5)$. To verify Proposition 2, we construct a baseline with $(w_1, w_2) = (0.3, 0.7)$. Fig. 9(b) depicts the performance with different w_i . Under optimal ST scheme, top-1 accuracy reaches 78 percent, whereas baseline accuracy is 69 percent. As a result, the ST guideline has a good impact on SlimFL's performance.

3) *Effectiveness of the Proposed Local Training Algorithm:* To configure out the superiority of the proposed local training algorithm (i.e., SUStain), we compare SUStain with SlimTrain [14] and USTrain [13] which are not only well known but also state-of-the-art SNN training algorithms. The two training algorithms are presented in **Algorithm 1** and **Algorithm 2**). We investigate the performance between training algorithm in the scheme with ten local devices and $\sigma^2 = -30\text{dB}$ in two data distributions (i.e., $\alpha = 0.1, 1.0$). As shown by experiments in Fig. 10(a), USTrain is unfit for SlimFL with high non-IID condition (i.e., $\alpha = 0.1$), where SlimTrain even outperforms USTrain. With IID data distribu-

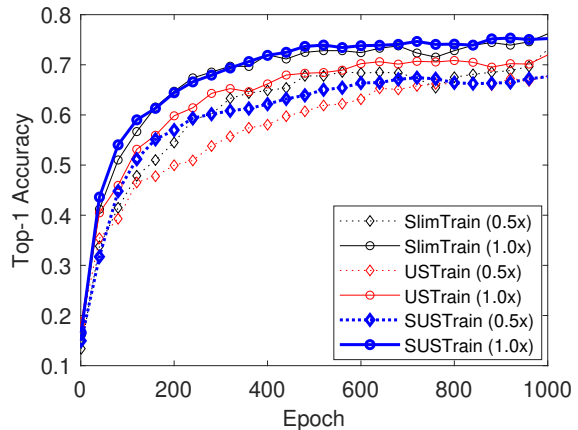
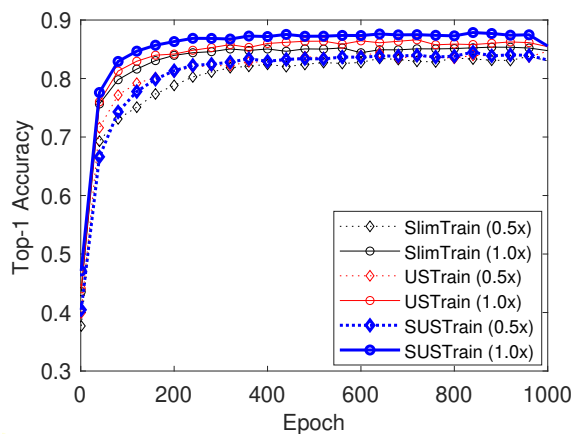
(a) Non-IID ($\alpha = 0.1$).(b) IID ($\alpha = 1.0$).

Fig. 10. Comparison of SNN training algorithms: SlimTrain [14], USTrain [13], and our proposed SUStain ($K = 10, \sigma^2 = -30\text{dB}$).

tion (i.e., $\alpha = 1.0$), USTrain outperforms SlimTrain. Fig. 10 corroborates that regardless of the data distributions, SUStain achieves high accuracy with fast convergence, as opposed to USTrain that is effective only under IID data distributions (i.e., $\alpha = 1.0$). We conjecture that the problem comes from the use of outdated teacher's knowledge in USTrain. In USTrain, the teacher's logit is set as the value before updating the teacher's model and is compared with a student after updating the teacher's model. Non-IID data distributions exacerbate this mismatch, where the full-width teacher model is significantly updated in the first epoch after downloading the global model due to the huge gap between local and global models.

D. Feasibility Studies on Channel and Training Environments

We investigate the generalization of SlimFL across various datasets and different number of local iterations in various channel model.

1) *Impact of Channel Models:* We design additional simulation to verify SlimFL works in more realistic channel models (e.g., Rician fading [30] and Two-wave with diffuse power fading (TWDP) [37]). In indoor wireless communication, Rician fading is superior than Rayleigh fading. In addition, TWDP is used in air, space or maritime wireless communication, where

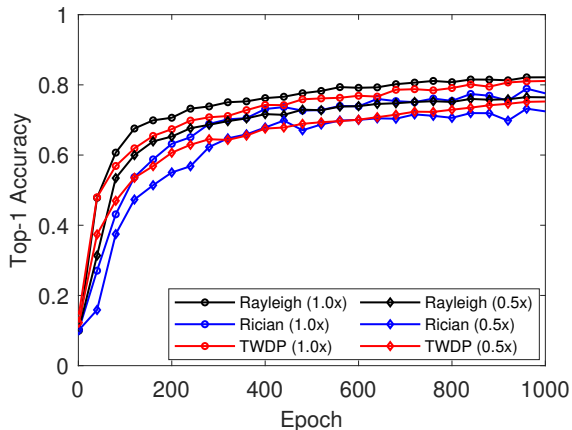


Fig. 11. Top-1 accuracy with the different fading effects.

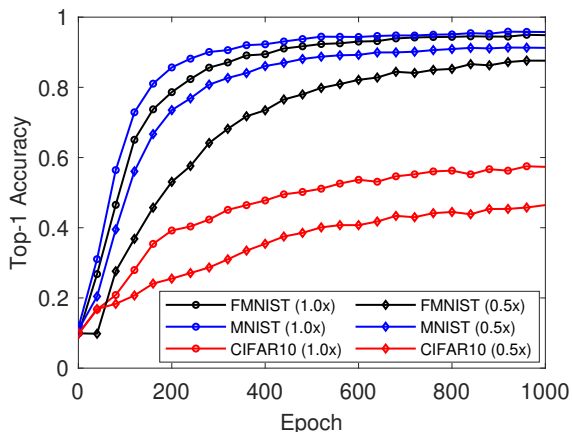
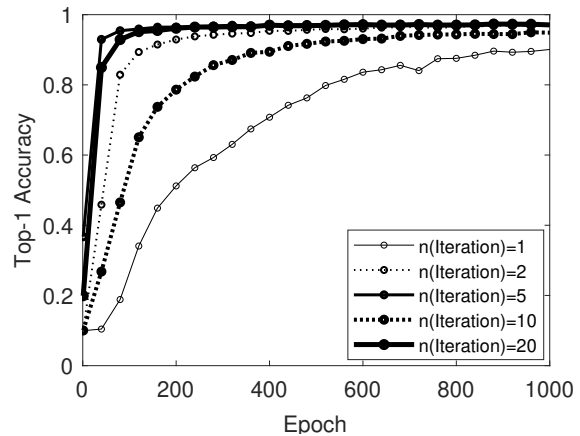


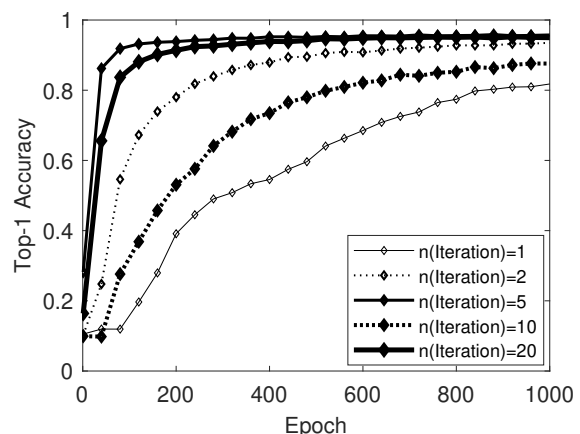
Fig. 12. Top-1 accuracy with the different datasets.

the channel fading is worse than Rayleigh [38]. We simulate Rician fading with K -factor 3.5, where the fading follows Rician distributions $\chi \sim \text{Rice}(0.5577, 0.2106)$. (K, Δ) -factor of TWDP fading is set to $(3.5, 0.1)$. All communication settings without fading effect is identical to Table II. Fig. 11 is the result of simulation. As shown in Fig. 11, the top-1 accuracy is found to be high in the order of Rayleigh fading, TWDP fading, and Rician fading channel models. SlimFL-1.0x always outperforms SlimFL-0.5x. Thus, SlimFL performs well in a variety of channel models.

2) *Impact of Datasets*: We conduct additional simulation to verify whether SlimFL operates with other dataset (e.g., CIFAR10 [39] and MNIST [40]). CIFAR10 dataset consists of 60,000 color images with size 32×32 . MNIST is handwritten digit classification dataset. It consists of 60,000 gray scale images with size 28×28 . Both image datasets have 10 classes, i.e., digits. CIFAR10 is known to be more challenging problem, which is harder than MNIST or FMNIST. The simulation is conducted with $\alpha = 1.0$, $K = 10$, and $\sigma^2 = -30\text{dB}$. Fig. 12 is the result of simulation. SlimFL with MNIST dataset shows the best top-1 accuracy, FMNIST data set shows the next highest accuracy, and CIFAR10 shows the lowest accuracy. In terms of the performance between 1.0x and 0.5x, SlimFL-



(a) SlimFL-1.0x.



(b) SlimFL-0.5x.

Fig. 13. Top-1 accuracy with different number of local iterations.

1.0x is always higher than SlimFL-0.5x. In other words, we confirm that our proposed SlimFL works well regardless of the dataset.

3) *Impact of Local Training Iterations*: This paper adopts local iterations per communication round as 1 for mathematical tractability. Thus, the convergence bound does not contain the local iteration. According to [24], the over-small or over-large local iterations cause high communication and computational cost, while the optimal local iteration exists. We conduct additional simulations to verify the SlimFL operation under different numbers of local iterations (i.e., 1, 2, 5, 10, and 20). As mentioned above, FedAvg does not guarantee that many local iterations is proportioned to the performance [32]. Similarly in our simulation as shown in Fig. 13, the top-1 accuracy of both SlimFL-1.0x and SlimFL-0.5x is high and is on the order of $\{5, 20, 2, 10, 1\}$. The empirical result shows that there exist at least two local extremums. One is located in $[2, 10]$, and the other is in $[5, \infty]$, respectively. In other words, there are at least two local optima corresponding to local iterations in $[1, \infty]$. Note that these local optima do not indicate global optima.

VII. CONCLUDING REMARKS

Existing FL solutions are incapable of adjusting flexibly to devices with varying amounts of available energy and channel throughput without jeopardizing communication or energy efficiency. To overcome this problem, we propose SlimFL, a novel framework for FL over SNNs that utilizes superpositioned training for local SNN training and superposition coding for trained model aggregation. Extensive analyses and simulations show that SlimFL is an energy- and communication-efficient solution in a variety of communication conditions and data distributions. SlimFL achieves higher accuracy and faster convergence while using less energy than vanilla FL, which requires 2X more communication resources. Additionally studying the impact of more adjustable SNN width levels could be an interesting topic for future work. Another interesting direction is to apply SlimFL for multitask learning in which various width configurations correspond to different tasks.

REFERENCES

- [1] H. Baek, W. J. Yun, Y. Kwak, S. Jung, M. Ji, M. Bennis, J. Park, and J. Kim, "Joint superposition coding and training for federated learning over multi-width neural networks," in *Proc. IEEE Conference on Computer Communications (INFOCOM)*, Virtual, May 2022.
- [2] S. Savazzi, M. Nicoli, M. Bennis, S. Kianoush, and L. Barbieri, "Opportunities of federated learning in connected, cooperative, and automated industrial systems," *IEEE Communications Magazine*, vol. 59, no. 2, pp. 16–21, February 2021.
- [3] N.-N. Dao, D. T. Ngo, N.-T. Dinh, T. V. Phan, N. D. Vo, S. Cho, and T. Braun, "Hit ratio and content quality tradeoff for adaptive bitrate streaming in edge caching systems," *IEEE Systems Journal*, vol. 15, no. 4, pp. 5094–5097, December 2021.
- [4] H. B. McMahan, E. Moore, D. Ramage, S. Hampson, and B. A. y Arcas, "Communication-efficient learning of deep networks from decentralized data," in *Proc. International Conference on Artificial Intelligence and Statistics (AISTATS)*, Fort Lauderdale, FL, USA, April 2017, pp. 1273–1282.
- [5] N. H. Tran, W. Bao, A. Y. Zomaya, M. N. H. Nguyen, and C. S. Hong, "Federated learning over wireless networks: Optimization model design and analysis," in *Proc. IEEE Conference on Computer Communications (INFOCOM)*, Paris, France, April 2019, pp. 1387–1395.
- [6] C. T. Dinh, N. H. Tran, M. N. H. Nguyen, C. S. Hong, W. Bao, A. Y. Zomaya, and V. Gramoli, "Federated learning over wireless networks: Convergence analysis and resource allocation," *IEEE/ACM Transactions on Networking*, vol. 29, no. 1, pp. 398–409, February 2021.
- [7] D. Kwon, J. Jeon, S. Park, J. Kim, and S. Cho, "Multiagent DDPG-based deep learning for smart ocean federated learning IoT networks," *IEEE Internet of Things Journal*, vol. 7, no. 10, pp. 9895–9903, October 2020.
- [8] T. Cover, "Broadcast channels," *IEEE Transactions on Information Theory*, vol. 18, no. 1, pp. 2–14, January 1972.
- [9] S. Han, H. Mao, and W. J. Dally, "Deep compression: Compressing deep neural networks with pruning, trained quantization and Huffman coding," in *Proc. International Conference on Learning Representations (ICLR)*, San Juan, Puerto Rico, May 2016.
- [10] G. E. Hinton, O. Vinyals, and J. Dean, "Distilling the knowledge in a neural network," in *Proc. the Conference on Neural Information Processing Systems (NeurIPS) Deep Learning and Representation Learning Workshop*, Montréal, Canada, December 2015, pp. 1–9.
- [11] D. Kim, J. Kim, J. Kwon, and T.-H. Kim, "Depth-controllable very deep super-resolution network," in *Proc. IEEE International Joint Conference on Neural Networks (IJCNN)*, Budapest, Hungary, July 2019.
- [12] H. Hu, D. Dey, M. Hebert, and J. A. Bagnell, "Learning anytime predictions in neural networks via adaptive loss balancing," in *Proc. AAAI Conference on Artificial Intelligence (AAAI)*, Honolulu, Hawaii, USA, January 2019, pp. 3812–3821.
- [13] J. Yu and T. S. Huang, "Universally slimmable networks and improved training techniques," in *Proc. IEEE/CVF International Conference on Computer Vision (ICCV)*, Seoul, South Korea, October 2019, pp. 1803–1811.
- [14] J. Yu, L. Yang, N. Xu, J. Yang, and T. Huang, "Slimmable neural networks," in *Proc. International Conference on Learning Representation (ICLR)*, New Orleans, LA, USA, May 2019.
- [15] C. Li, G. Wang, B. Wang, X. Liang, Z. Li, and X. Chang, "Dynamic slimmable network," in *Proc. IEEE/CVF Conference on Computer Vision and Pattern Recognition (CVPR)*, Virtual, June 2021, pp. 8607–8617.
- [16] F. Yang, L. Herranz, Y. Cheng, and M. G. Mozerov, "Slimmable compressive autoencoders for practical neural image compression," in *Proceedings of the IEEE/CVF Conference on Computer Vision and Pattern Recognition*, 2021, pp. 4998–5007.
- [17] Z. Wu, D. Zhao, Q. Liang, J. Yu, A. Gulati, and R. Pang, "Dynamic sparsity neural networks for automatic speech recognition," in *Proc. IEEE International Conference on Acoustics, Speech and Signal Processing (ICASSP)*, 2021, pp. 6014–6018.
- [18] B. McMahan and D. Ramage, "Federated learning: Collaborative machine learning without centralized training data," *Google AI Blog*, April 2017.
- [19] X. Li, M. Jiang, X. Zhang, M. Kamp, and Q. Dou, "FedBN: Federated learning on non-IID features via local batch normalization," in *Proc. International Conference on Learning Representations (ICLR)*, Virtual, May 2021.
- [20] T. Li, A. K. Sahu, M. Zaheer, M. Sanjabi, A. Talwalkar, and V. Smith, "Federated optimization in heterogeneous networks," *Proc. Machine Learning and Systems (MLSys)*, vol. 2, pp. 429–450, 2020.
- [21] J. Wang, Z. Charles, Z. Xu, G. Joshi, H. B. McMahan, M. Al-Shedivat, G. Andrew, S. Avestimehr, K. Daly, D. Data *et al.*, "A field guide to federated optimization," *arXiv preprint, abs/2107.06917*, July 2021.
- [22] A. Khaled, K. Mishchenko, and P. Richtárik, "Tighter theory for local SGD on identical and heterogeneous data," in *Proc. International Conference on Artificial Intelligence and Statistics (AISTATS)*, Palermo, Sicily, Italy, August 2020, pp. 4519–4529.
- [23] L. Mangasarian, "Parallel gradient distribution in unconstrained optimization," *SIAM Journal on Control and Optimization (SICON)*, vol. 33, no. 6, pp. 1916–1925, November 1995.
- [24] X. Li, K. Huang, W. Yang, S. Wang, and Z. Zhang, "On the convergence of FedAvg on non-iid data," in *Proc. International Conference on Learning Representation (ICLR)*, Addis Ababa, Ethiopia, April 2020.
- [25] A. Mohtashami, M. Jaggi, and S. U. Stich, "Simultaneous training of partially masked neural networks," *arXiv preprint, abs/2106.08895*, June 2021.
- [26] D. N. C. Tse and P. Viswanath, *Fundamentals of Wireless Communications*. Cambridge University Press, 2005.
- [27] Z. Ding, Y. Liu, J. Choi, Q. Sun, M. Elkashlan, I. Chih-Lin, and H. V. Poor, "Application of non-orthogonal multiple access in LTE and 5G networks," *IEEE Communications Magazine*, vol. 55, no. 2, pp. 185–191, February 2017.
- [28] V. D. Tuong, T. P. Truong, T.-V. Nguyen, W. Noh, and S. Cho, "Partial computation offloading in NOMA-assisted mobile-edge computing systems using deep reinforcement learning," *IEEE Internet of Things Journal*, vol. 8, no. 17, pp. 13 196–13 208, September 2021.
- [29] A. G. Howard, M. Zhu, B. Chen, D. Kalenichenko, W. Wang, T. Weyand, M. Andreetto, and H. Adam, "Mobilenets: Efficient convolutional neural networks for mobile vision applications," *arXiv preprint arXiv:1704.04861*, April 2017.
- [30] A. F. Molisch, *Wireless Communications*, 2nd ed. Wiley, 2011.
- [31] J. Choi, "Joint rate and power allocation for NOMA with statistical CSI," *IEEE Transactions on Communications*, vol. 65, no. 10, pp. 4519–4528, October 2017.
- [32] H. Wang, M. Yurochkin, Y. Sun, D. S. Papailiopoulos, and Y. Khazaeni, "Federated learning with matched averaging," in *Proc. International Conference on Learning Representation (ICLR)*, Virtual, May 2020.
- [33] S. U. Stich, "Local SGD converges fast and communicates little," in *Proc. International Conference on Learning Representations (ICLR)*, Vancouver, BC, Canada, April/May 2018.
- [34] H. Xiao, K. Rasul, and R. Vollgraf, "Fashion-mnist: a novel image dataset for benchmarking machine learning algorithms," *arXiv preprint, abs/1708.0774*, August 2017.
- [35] T. H. Hsu, H. Qi, and M. Brown, "Measuring the effects of non-identical data distribution for federated visual classification," *Proc. the Conference on Neural Information Processing Systems (NeurIPS) Federated Learning for Data Privacy and Confidentiality Workshop*, September 2019.
- [36] D. Hernandez and T. B. Brown, "Measuring the algorithmic efficiency of neural networks," *arXiv preprint, abs/2005.04305*, May 2020.

- [37] G. Durgin, T. Rappaport, and D. de Wolf, "New analytical models and probability density functions for fading in wireless communications," *IEEE Transactions on Communications*, vol. 50, no. 6, pp. 1005–1015, 2002.
- [38] C.-X. Wang, J. Huang, H. Wang, X. Gao, X. You, and Y. Hao, "6g wireless channel measurements and models: Trends and challenges," *IEEE Vehicular Technology Magazine*, vol. 15, no. 4, pp. 22–32, December 2020.
- [39] A. Krizhevsky, V. Nair, and G. Hinton, "Cifar-10 (canadian institute for advanced research)." [Online]. Available: <http://www.cs.toronto.edu/~kriz/cifar.html>
- [40] L. Deng, "The mnist database of handwritten digit images for machine learning research," *IEEE Signal Processing Magazine*, vol. 29, no. 6, pp. 141–142, November 2012.

APPENDIX A PROOF OF THEOREM 1

A. Proof of Lemma 1

Proof. According to f_t in (10) and Assumption 3,

$$\|f_t - \bar{f}_t\|^2 = \left\| \frac{1}{Kp_1} \sum_{k \in \text{HUF}} (g_t^k - \bar{g}_t^k) \odot \Xi + \frac{1}{Kp_2} \sum_{k \in \text{F}} (g_t^k - \bar{g}_t^k) \odot \Xi^{-1} \right\|^2 \quad (23)$$

$$\leq \frac{2}{Kp_1} \sum_{k \in \text{H}} \|(g_t^k - \bar{g}_t^k) \odot \Xi\|^2 + \frac{2}{Kp_2} \sum_{k \in \text{F}} \|(g_t^k - \bar{g}_t^k) \odot \Xi^{-1}\|^2 \quad (24)$$

$$\leq \frac{2}{Kp_1} \sum_{k \in \text{H}} \|g_t^k - \bar{g}_t^k\|^2 + \frac{2}{Kp_2} \sum_{k \in \text{F}} \|g_t^k - \bar{g}_t^k\|^2, \quad (25)$$

where the first inequality follows from the Cauchy–Schwarz (C-S) inequality, and the last step is because $\|X \odot \Xi\|^2 \leq \|X\|^2$. Similarly, we have

$$\|g_t^k - \bar{g}_t^k\|^2 = \left\| \sum_{i=1}^2 w_i (\nabla F^k(\theta_t, \zeta_t^k) - \nabla F^k(\theta_t)) \odot \Xi_i \right\|^2 \leq 2 \sum_{i=1}^2 w_i^2 \|\nabla F^k(\theta_t, \zeta_t^k) - \nabla F^k(\theta_t)\|^2. \quad (26)$$

Taking an expectation at both sides yields

$$\mathbb{E}\|g_t^k - \bar{g}_t^k\|^2 \leq 2\sigma_k^2 \sum_{i=1}^2 w_i^2. \quad (27)$$

Combining (25) and (27) finalizes the proof. \square

B. Proof of Lemma 2

Proof. According to (10), we have

$$\|\theta_{t+1} - \theta^*\|^2 = \|\theta_t - \eta_t f_t - \theta^* - \eta_t \bar{f}_t + \eta_t \bar{f}_t\|^2 \quad (28)$$

$$\begin{aligned} &= \underbrace{\|\theta_t - \theta^* - \eta_t \bar{f}_t\|^2}_{A_1} \\ &\quad + 2\eta_t \underbrace{\langle \theta_t - \theta^* - \eta_t f_t, \bar{f}_t - f_t \rangle}_{A_2} + \underbrace{\eta_t^2 \|f_t - \bar{f}_t\|^2}_{A_3} \quad (29) \\ &= \|\theta_t - \theta_t^*\|^2 - \underbrace{2\eta_t \langle \theta_t - \theta^*, \bar{f}_t \rangle}_{B_1} + \underbrace{\eta_t^2 \|\bar{f}_t\|^2}_{B_2} \\ &\quad + A_2 + A_3. \quad (30) \end{aligned}$$

Here, $\mathbb{E}[A_2] = 0$ due to $\mathbb{E}(f_t) = \bar{f}_t$, and A_3 is bounded according to Lemma 1. Note that $\bar{f}_t = \mathbb{E}[f_t] = \mathbb{E}[\nabla F(\theta_t)] = \nabla \mathbb{E}[F(\theta_t)]$, and $\mathbb{E}[F]$ inherits the μ -strong convexity and L -smoothness from F . By the L -smoothness of $\mathbb{E}[F]$, we have

$$\|\bar{f}_t\|^2 \leq 2L(\mathbb{E}[F(\theta_t)] - F(\theta^*)), \quad (31)$$

showing the boundness of B_2 . Next, by the μ -strong convexity of $\mathbb{E}[F]$, we have

$$\langle \theta^* - \theta_t, \bar{f}_t \rangle \leq \mathbb{E}[F(\theta^*) - F(\theta_t)] - \frac{\mu}{2} \|\theta_t - \theta^*\|^2, \quad (32)$$

proving the boundness of B_1 . Applying the bounds of B_1 and B_2 , we obtain

$$A_1 \leq (1 - \mu\eta_t) \|\theta_t - \theta^*\|^2 - 2\eta_t(1 - L\eta_t) \mathbb{E}[F(\theta_t) - F(\theta^*)], \quad (33)$$

where the last term on the RHS vanishes for $\eta_t < \frac{1}{L}$. Taking the expectation at both sides completes the proof. \square

C. Completing the Proof of Theorem 1

Proof. Since $\eta_t = \frac{2}{\mu t + 2L - \mu} \leq \frac{1}{L}$, applying Lemma 2, we have

$$\Delta_{t+1} \leq (1 - \mu\eta_t) \Delta_t + \eta_t^2 B. \quad (34)$$

By induction, we aim to show that $\Delta_t \leq \frac{v}{t + 2\kappa - 1}$ where $\kappa = \frac{L}{\mu}$ and $v = \max\{2\kappa\Delta_1, 4B/\mu^2\}$ as elaborated next. By the definition of v , it is trivial that $\Delta_1 \leq \frac{v}{2\kappa}$. Assuming that $\Delta_{t'} \leq \frac{v}{t' + 2\kappa - 1}$ holds, we have

$$\Delta_{t'+1} \leq (1 - \mu\eta_{t'}) \Delta_{t'} + \eta_{t'}^2 B \quad (35)$$

$$\leq \left(1 - \frac{2}{t' + 2\kappa - 1}\right) \frac{v}{t' + 2\kappa - 1} + \frac{4B/\mu^2}{(t' + 2\kappa - 1)^2} \quad (36)$$

$$= \frac{(t' + 2\kappa - 2)v - (v - 4B/\mu^2)}{(t' + 2\kappa - 1)^2} \quad (37)$$

$$\leq \frac{t' + 2\kappa - 2}{(t' + 2\kappa - 1)^2} v \leq \frac{v}{t' + 2\kappa}, \quad (38)$$

which proves that $\Delta_t \leq \frac{v}{t + 2\kappa - 1}$. For $t = 1$, we obtain

$$v = \max\{2\kappa\Delta_1, \frac{4B}{\mu^2}\} \leq 2\kappa\Delta_1 + \frac{4B}{\mu^2}. \quad (39)$$

Finally, by the L -Smoothness of F , one has

$$\mathbb{E}[F(\theta_t)] - F^* = \mathbb{E}[F(\theta_t) - F(\theta^*)] \leq \frac{L}{2} \mathbb{E}\|\theta_t - \theta^*\|^2. \quad (40)$$

Applying Lemma 2 with the results above, we have

$$\mathbb{E}\|\theta_t - \theta^*\|^2 \leq \frac{v}{t + 2\kappa - 1} \leq \frac{2}{\mu} \cdot \frac{\mu L \Delta_1 + 2B}{\mu t + 2L - \mu}, \quad (41)$$

which completes the proof of the theorem. \square



Won Joon Yun is currently a Ph.D. student in electrical and computer engineering at Korea University, Seoul, Republic of Korea, since March 2021, where he received his B.S. in electrical engineering. His current research interests include multi-agent deep reinforcement learning for various mobile and network systems.

He was a recipient of the Best Paper Awards by KICS (2020–2021) and IEEE ICOIN Best Paper Award (2021).



Yunseok Kwak is currently a Ph.D. student in electrical and computer engineering at Korea University, Seoul, Republic of Korea, since March 2021. He received his B.S. in mathematics from Yonsei University, Seoul, Republic of Korea, in 2021. His research interests include multi-agent deep reinforcement learning and quantum machine learning.

He was a recipient of IEEE Vehicular Technology Society (VTS) Seoul Chapter Award (2021).



Hankyul Baek is currently a Ph.D. student in electrical and computer engineering at Korea University, Seoul, Republic of Korea, since March 2021. He received his B.S. in electrical engineering from Korea University, Seoul, Republic of Korea, in 2020. He was with LG Electronics, Seoul, Republic of Korea, from 2020 to 2021. His current research interests include multi-agent deep reinforcement learning and its augmented reality applications.



Soyi Jung (Member, IEEE) has been an assistant professor at the School of Software, Hallym University, Chuncheon, Republic of Korea, since September 2021. She also holds a visiting scholar position at Donald Bren School of Information and Computer Sciences, University of California, Irvine, CA, USA, from 2021 to 2022. She was a research professor at Korea University, Seoul, Republic of Korea, during 2021. She received her B.S., M.S., and Ph.D. degrees from Ajou University, Suwon, Republic of Korea, in 2013, 2015, and 2021, respectively.

She was a recipient of Bronze Paper Award from IEEE Seoul Section Student Paper Contest (2018), IEEE ICOIN Best Paper Award (2021), and IEEE Vehicular Technology Society (VTS) Seoul Chapter Award (2021).



Mingyue Ji (Member, IEEE) received the B.E. degree in communication engineering from Beijing University of Posts and Telecommunications, China, in 2006, the M.Sc. degree in electrical engineering from the Royal Institute of Technology, Sweden, in 2008, the M.Sc. degree in electrical engineering from the University of California at Santa Cruz, in 2010, and the Ph.D. degree from the Ming Hsieh Department of Electrical Engineering, University of Southern California, in 2015. From 2015 to 2016, he was a Staff II System Design Scientist with

Broadcom Corporation. He is currently an Assistant Professor with the Electrical and Computer Engineering Department, The University of Utah.

He received the IEEE Communications Society Leonard G. Abraham Prize for the Best IEEE Journal on Selected Areas in Communications Paper in 2019, the Best Paper Award in IEEE GLOBECOM 2021 Conference, the Best Paper Award in IEEE ICC 2015 Conference, the Best Student Paper Award in IEEE European Wireless 2010 Conference, and the USC Annenberg Fellowship from 2010 to 2014. Since 2020, he has been serving as an Associate Editor for IEEE Transactions on Communications.



Mehdi Bennis (Fellow, IEEE) is a tenured Full Professor with the Centre for Wireless Communications, University of Oulu, Finland, an Academy of Finland Research Fellow, and the Head of the Intelligent Connectivity and Networks/Systems Group (ICON). He has published more than 200 research papers in international conferences, journals, and book chapters. His main research interests are in radio resource management, heterogeneous networks, game theory, and distributed machine learning in 5G networks and beyond.

He has been the recipient of several prestigious awards, including the 2015 Fred W. Ellersick Prize from the IEEE Communications Society, the 2016 Best Tutorial Prize from the IEEE Communications Society, the 2017 EURASIP Best Paper Award for the Journal of Wireless Communications and Networks, the All-University of Oulu Award for research, the 2019 IEEE ComSoc Radio Communications Committee Early Achievement Award, and the 2020 Clarivate Highly Cited Researcher by the Web of Science. He is an Editor of IEEE Transactions on Communications and the Specialty Chief Editor of Data Science for Communications in the Frontiers in Communications and Networks.



Jihong Park (Senior Member, IEEE) received the B.S. and Ph.D. degrees from Yonsei University, South Korea. He is currently a Lecturer (Assistant Professor) with the School of Information Theory, Deakin University, Australia. His research interests include ultra-dense/ultra-reliable/mmWave system designs, and distributed learning/control/ledger technologies and their applications for beyond-5G/6G communication systems. He served as a Conference/Workshop Program Committee Member for IEEE GLOBECOM, ICC, and WCNC, and for

NeurIPS, ICML, and IJCAI. He is an Associate Editor of Frontiers in Data Science for Communications, and a Review Editor of Frontiers in Aerial and Space Networks.



Joongheon Kim (Senior Member, IEEE) has been with Korea University, Seoul, Korea, since September 2019, and he is currently an associate professor at the School of Electrical Engineering. He received the B.S. and M.S. degrees from Korea University, Seoul, Korea, in 2004 and 2006, respectively; and the Ph.D. degree in computer science from the University of Southern California (USC), Los Angeles, CA, USA, in 2014. Before joining Korea University, he was with LG Electronics, Seoul, Korea, from 2006 to 2009; InterDigital, San Diego, CA, USA, in 2012; Intel Corporation, Santa Clara in Silicon Valley, CA, USA, from 2013 to 2016; and Chung-Ang University, Seoul, Korea, from 2016 to 2019.

He is a senior member of the IEEE and serves as an editor for *IEEE Transactions on Vehicular Technology*, *IEEE Communications Standards Magazine*, and *Computer Networks (Elsevier)*. He is also a distinguished lecturer for *IEEE Communications Society* (2022–2023). He was a recipient of the Annenberg Graduate Fellowship with his Ph.D. admission from USC (2009), Intel Corporation Next Generation and Standards (NGS) Division Recognition Award (2015), Paper Awards from IEEE Seoul Section Student Paper Contests (2019 and 2020), *IEEE Systems Journal* Best Paper Award (2020), IEEE ICOIN Best Paper Award (2021), and IEEE Vehicular Technology Society (VTS) Seoul Chapter Awards (2019 and 2021).